Materials and Design 167 (2019) 107637

Contents lists available at ScienceDirect

Materials and Design

journal homepage: www.elsevier.com/locate/matdes

Sound absorption performance of the acoustic absorber fabricated by compression and microperforation of the porous metal

Panfeng Bai [a], Xiaocui Yang [a], Xinmin Shen [a,b,*], Xiaonan Zhang [a,**], Zhizhong Li [a], Qin Yin [a], Guoliang Jiang [a], Fei Yang [a]

[a] *Department of Mechanical Engineering, College of Field Engineering, Army Engineering University, No. 1 Haifu Street, Nanjing, Jiangsu 210007, China*
[b] *State Key Laboratory in Ultra-precision Machining Technology, Department of Industrial and Systems Engineering, The Hong Kong Polytechnic University, Kowloon, Hong Kong, China*

HIGHLIGHTS

- Novel acoustic absorber was developed for better sound absorption by compression and microperforation of porous metal.
- The compressed and microperforated porous metal panel absorber could achieve better sound absorbing coefficient.
- The constructed semi-empirical model was validated to achieve optimal acoustic absorber by two replication experiments.
- Micromorphology of the proposed acoustic absorber gave intuitive explanations for its sound absorption performance.

GRAPHICAL ABSTRACT

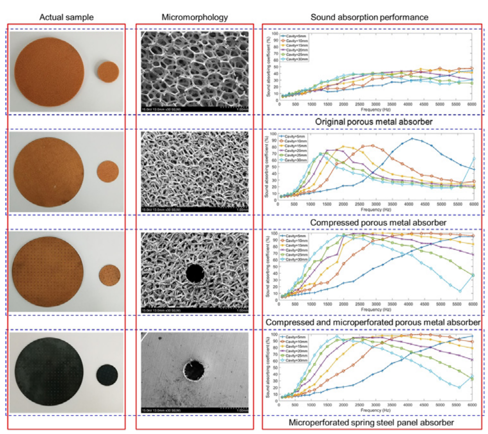

ARTICLE INFO

Article history:
Received 10 December 2018
Received in revised form 22 January 2019
Accepted 3 February 2019
Available online 5 February 2019

Keywords:
Sound absorption performance
Porous metal
Compression
Microperforation
Superposition absorption effect
Micromorphology

ABSTRACT

Novel acoustic absorbers were fabricated by the compression and microperforation of the porous metal, which aimed to develop practical acoustic absorbers for the noise reduction. Sound absorbing coefficients of the five investigated acoustic absorbers were measured by the AWA6128A detector according to the standing wave method, and their trends were consistent with normal sound absorption principle of the porous metal absorber and that of the microperforated panel absorber. The results proved that with same length of the cavity, sound absorption performance could be obviously improved by the compression and microperforation. When length of the cavity was 20 mm, average sound absorbing coefficient of the compressed and microperforated porous metal panel absorber in frequency range 100–6000 Hz reached 59.69%, which was superior to that 25.70% of original porous metal absorber and that 31.49% of the microperforated spring steel panel absorber. In the constructed semi-empirical model, a fourth-order polynomial function was treated as the coupling function to express the superposition absorption effect, and its veracity and reliability was validated by two replication experiments. Micromorphology of the compressed and microperforated porous metal panel provided the intuitive explanations to the improvement of its sound absorption performance.

* Correspondence to: X. Shen, Department of Mechanical Engineering, College of Field Engineering, Army Engineering University, No. 1 Haifu Street, Nanjing, Jiangsu 210007, China.
** Corresponding author.
E-mail addresses: shenxmjfjlgdx2014@163.com (X. Shen), zxn8206@163.com (X. Zhang).

https://doi.org/10.1016/j.matdes.2019.107637

1. Introduction

Noise pollution, air pollution, water pollution, and solid waste pollution were considered as the four major environmental problems all over the world [1,2]. The noise can result in pathological changes to auditory organ, visual organ, internal organ, and central nervous system of the human and animals [3,4]. Along with the development of advanced material and precision manufacturing, many acoustic metamaterials have been proposed, which aim to reduce the increasingly serious noise pollution [5–10]. Acoustic metasurface with hybrid resonances was developed by Ma et al. [5,6], which could achieve robust impedance matching and a perfect absorption in characteristic frequency. Composite 3D-printed metastructure was fabricated by Matlack et al. [7], which could obtain low-frequency and broadband vibration absorption. Hilbert fractal acoustic metamaterials (HFAMMs) with self-similar fractal structure was prepared by Zhao et al. [8], which was proved to be effective in the transformer noise reduction. A novel ultrathin Ashoka Chakra like acoustic metastructure was reported by Kumar et al. [9], which could demonstrate broad bandwidth and high absorption characteristics. The layered acoustic metamaterial which included two critically coupled membrane-type acoustic metamaterials sandwiching a porous material layer was proposed by Wang et al. [10], and it could obtain perfect absorption at 312 Hz with thickness of 15 mm. however, fabrication of these acoustic metamaterials is high-cost and time-consuming, because their structures are complicated and their accuracies are high, which limit their large-scale practical applications in the noise reduction field. Meanwhile, these acoustic metamaterials are inherently constrained by the narrow frequency band character and hence are somewhat limited in their usefulness [11]. Therefore, development of the practical acoustic absorber with low-cost and simple fabrication process is still challenge for the researchers around the world and research focus in the noise reduction field.

Microperforated metal panel and porous metal are two common materials used in the noise reduction, and both of them have the advantages of a low manufacturing cost, excellent machinability, fine fire resistance, high strength, and convenient for transportation, installation, application and maintenance [12–17], which make them the promising candidates for practical acoustic absorber in noise reduction field. A perforated composite panel utilizing recycled rubber was developed by Xu et al. [12], and it was proved to be efficient for sound absorption especially for frequency domain lower than 1000 Hz. The multiple-layer microperforated panels were fabricated and investigated by Bucciarelli et al. for broadband sound absorption at low frequency [13]. The cellular titanium foam and reticular titanium foam were prepared by Liu et al. through slurry-immersed sintering for excellent sound absorption performance [14]. Modelling and optimization of sound absorption in replicated microcellular metals were conducted by Otaru et al. according to Wilson's poroacoustic model [15]. Acoustic absorption of a 3D printed microperforated panel backed by a porous material was experimentally measured by Liu et al. [16], and the obtained measurement results agreed fairly well with the theoretical model. Absorption properties of the thin microperforated partitions lined with anisotropic fibrous materials were examined by Bravo and Colina [17]. These researches on the investigation and optimization of sound absorption performance of the microperforated panel, or the porous material, or composite of them two promote their applications in noise reduction field. In particular, the composite structure of these two materials could obtain a high sound absorbing coefficient and wide absorption band, which is obviously superior to the single absorber with the same total thickness. Therefore, developing the composite acoustic absorber is main trend in the noise reduction field.

Optimization of structural parameters of the composite acoustic absorber is critical step to realize the practical perfect acoustic absorber. Taken the practical application into consideration, the composite acoustic absorber will be more practical when its total thickness is smaller, because it is propitious to reduce the costs in fabrication, transportation, installation, application, and maintenance. Moreover, it will be better if structure of the composite acoustic absorber is simple, although this conflicts with the common knowledge that more complex structure generates better sound absorption performance. Fortunately, it had been proved that sound absorption efficiency of the porous metal was improved by the compression, and thickness of the compressed porous metal could be below 1 mm [18], which indicated that the compressed porous metal was potential to be treated as plate in the microperforated panel. According to this method, acoustic absorber fabricated by compression and microperforation of the porous metal was proposed, which combined the porous metal and the microperforated panel into one absorber. The utilized porous copper was prepared with the electrodeposition method [19], and it was compressed by universal testing machine and further microperforated by spark-erosion drilling [20]. Sound absorption performance of the propose acoustic absorber with different cavities was measured based on standing wave method [21]. Simultaneously, sound absorption performances of the original porous metal, the compressed porous metal, the microperforated spring steel panel, and the microperforated uncompressed porous metal were also measured for contrast. Afterwards, theoretical analysis on sound absorbing coefficient of the compressed and microperforated porous metal panel absorber was conducted based on the Johnson-Champoux-Allard model [22] and Maa's theory [23], and a fourth-order polynomial function was treated as coupling function to describe the superposition absorption effect of porous structures and microperforated structures in the compressed and microperforated porous metal panel absorber. Micromorphology of the proposed acoustic absorber was investigated by the scanning electron microscope, which supplied intuitive evidences to explain the reason for amelioration in sound absorption.

2. Materials and measurement

The utilized porous metal used in this study was porous copper, as shown in Fig. 1(a). Its structural parameters, which included thickness d_p, porosity ϕ, and static flow resistivity σ, were 5 mm, 90%, and 9524 $\text{Pa}\cdot\text{s}\cdot\text{m}^{-2}$, respectively. The thickness d_p was measured by the vernier caliper. The porosity ϕ was calculated by the Eq. (1). Here ρ_1 is density of the metal, which is measured by drainage method; M is mass of the porous metal sample, which is measured by electronic balance; ρ_2 was density of the porous metal; V was volume of the porous metal sample, which can be obtained by measuring its diameter and thickness. The static flow resistivity σ was measured by water tank method, which was calculated by the Eq. (2). Here Δp is pressure difference between two surfaces of the sample; v is velocity of the flow in the sample; t is thickness of the sample.

$$\phi = \left(1 - \frac{\rho_2}{\rho_1}\right) \cdot 100\% = \left(1 - \frac{M}{V} \cdot \frac{1}{\rho_1}\right) \cdot 100\% \tag{1}$$

$$\sigma = \frac{\Delta p}{vt} \tag{2}$$

Afterwards, the porous metal was extruded with the CTM2050 universal testing machine (Wuxi City Bleecker Trading Co., Ltd., Wuxi, Jiangsu, China) with pressure 10 kN [18]. After the compression, thickness of the sample was reduced from original 5 mm to 0.5 mm, as shown in Fig. 1(b). Later, the sample was further microperforated by the spark-erosion drilling [20], and it was shown in Fig. 1(c). Distribution of the holes in this microperforated sample was square array, and diameter of the hole d and distance between the neighbor holes b were 0.75 mm and 4.5 mm, respectively.

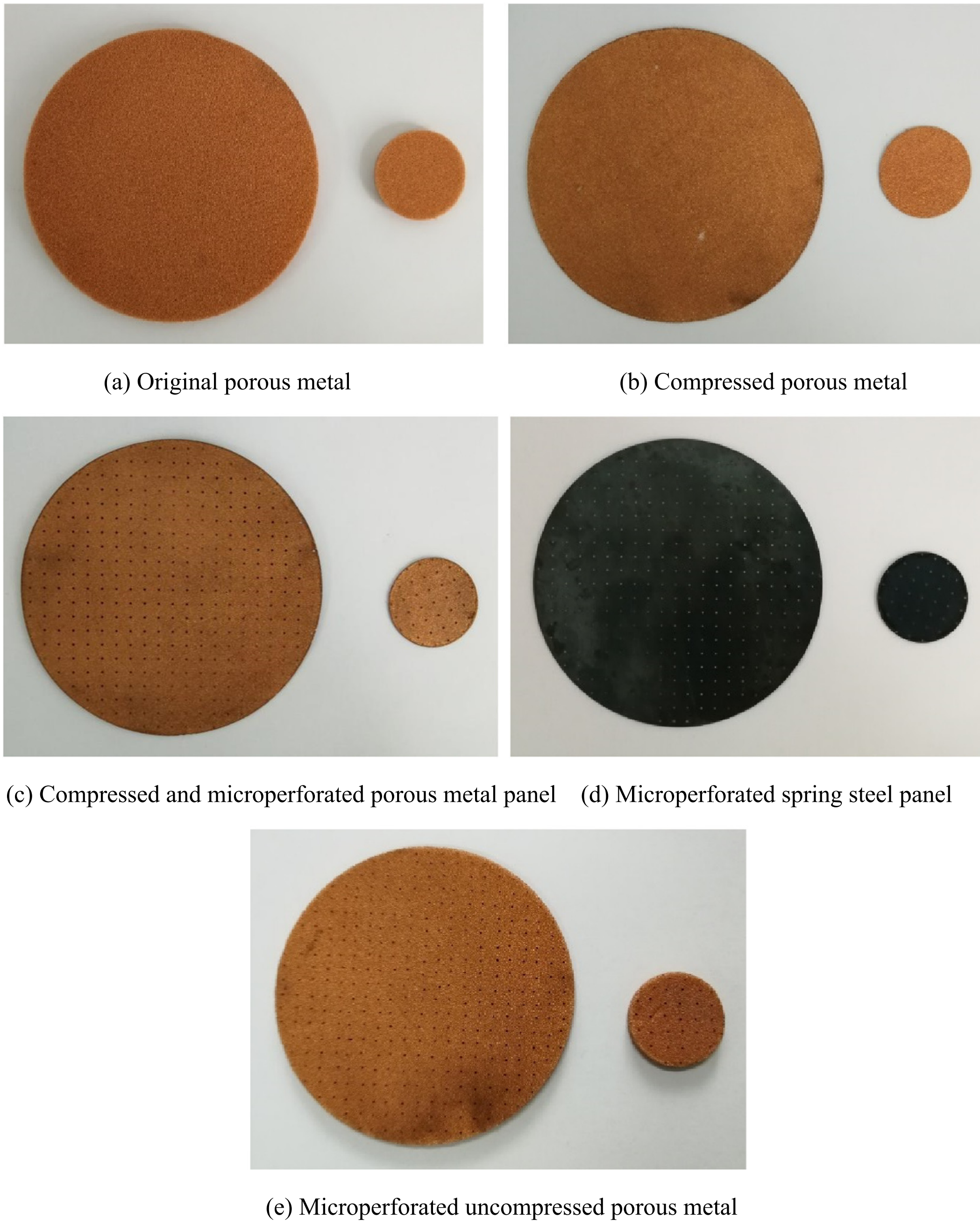

Fig. 1. Actual pictures of the five prepared samples.

It could be calculated based on the Eq. (3) that the perforating rate ε was 2.18%, which satisfied the common requirement of 1%–3% for the perforating rate in usual microperforated panel absorber [24].

$$\varepsilon = \frac{\pi}{4}\left(\frac{d}{b}\right)^2 \tag{3}$$

Meanwhile, a microperforated spring steel panel was also prepared for contrast, as shown in Fig. 1(d). Its parameters, such as thickness of the panel, diameter of the hole, and distance between neighbor holes, were entirely consistent with those of the compressed and microperforated porous metal panel absorber respectively. Moreover, the original porous metal in Fig. 1(a), the compressed porous metal without the microperforation in Fig. 1(b), and the microperforated uncompressed porous metal in Fig. 1(e) were treated as the contrasts. Sound absorption in the compressed and microperforated porous metal panel was superposition absorption effect of porous structures and microperforated structures. Therefore, conductions of the control experiments aimed to compare contribution degrees of these two structures and check the distribution of superposition absorption effect.

Sound absorbing coefficients of the samples with different cavities were measured by AWA6128A detector (Hangzhou Aihua Instruments Co., Ltd., Zhejiang, China) based on standing wave method [21], and Schematic diagram of the detection system was shown in Fig. 2. The sample was installed in the sample fixer, and length of the postposition cavity was controlled by the cavity adjuster. The audio power signal was supplied by the workstation and given to the loudspeaker box, which was transformed to plane wave in the standing wave tube. The plane wave was reflected by the sample, which resulted in standing wave field in the tube. Maximal value and minimal value of the sound pressure were measured by the acoustic probe, and the sound absorbing coefficient in the normal incidence was calculated by the software in the

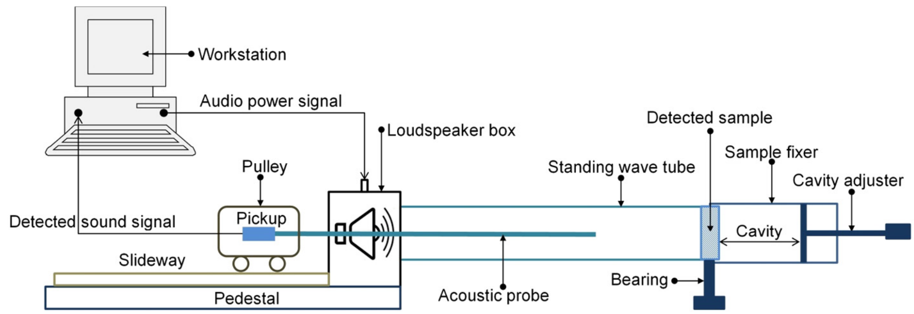

Fig. 2. Schematic diagram of the AWA6128A detector.

workstation [18,21]. According to the requirements in GB/T 18696.1-2004 and ISO 10534-1:1996, the sample with diameter of 96 mm was measured for sound absorbing coefficients in the frequency range of 90–2075 Hz, and that with diameter of 30 mm was measured for sound absorbing coefficients in the frequency range of 1500–6640 Hz [18,21]. Thus, taking testing accuracy and measurement capability of the equipment into consideration, the measured sound frequencies were 100 Hz, 200 Hz, 300 Hz, 400 Hz, 500 Hz, 600 Hz, 700 Hz, 800 Hz, 950 Hz, 1100 Hz, 1300 Hz, 1500 Hz, 1800 Hz, 2000 Hz, 2300 Hz, 2600 Hz, 2900 Hz, 3200 Hz, 3500 Hz, 3800 Hz, 4100 Hz, 4400 Hz, 4700 Hz, 5000 Hz, 5300 Hz, 5600 Hz, and 6000 Hz, which included 27 frequency points. In order to reduce the test error, each test was repeated by 10 times, and it was also the requirement marked in the instruction of the detector. Following this scheme, the five prepared samples, which included the original porous metal, the compressed porous metal, the compressed and microperforated porous metal panel,

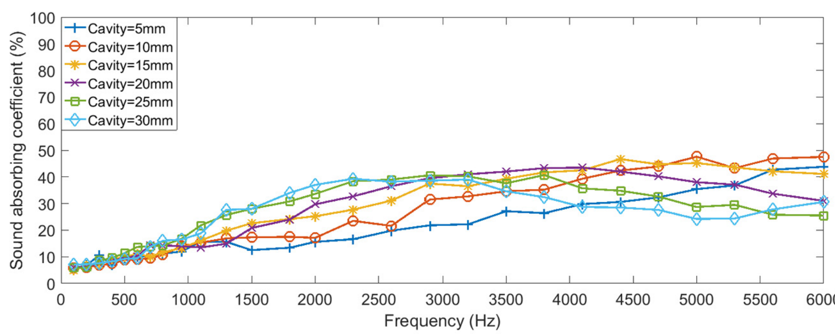

(a) The original porous metal

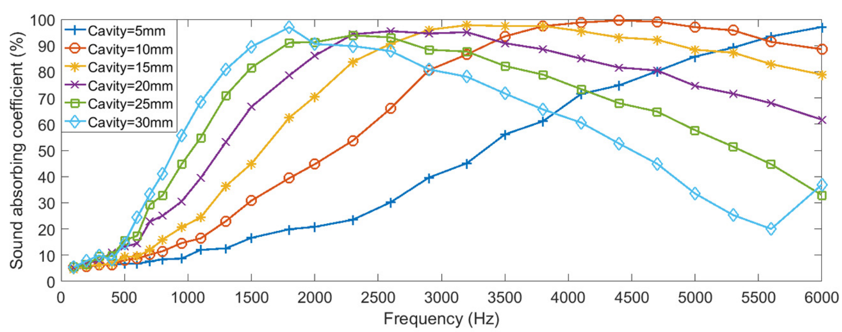

(b) The compressed porous metal

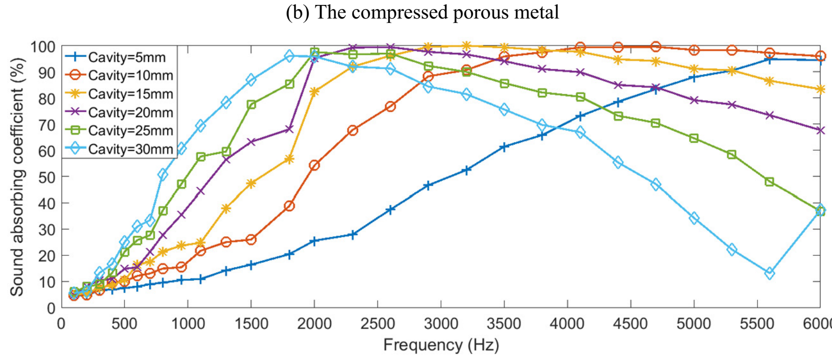

(c) The compressed and microperforated porous metal panel

Fig. 3. Distributions of sound absorbing coefficients of the five samples with different cavities.

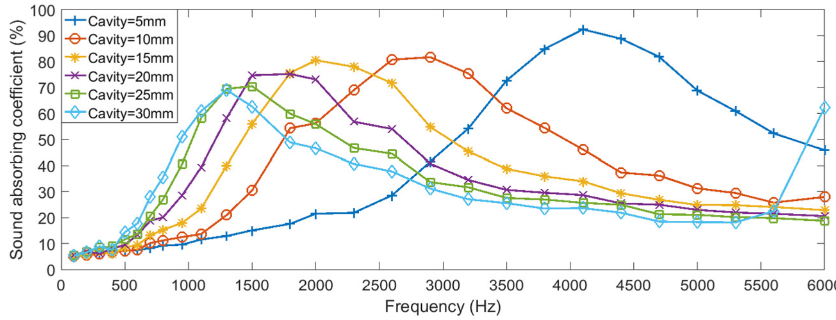

(d) The microperforated spring steel panel

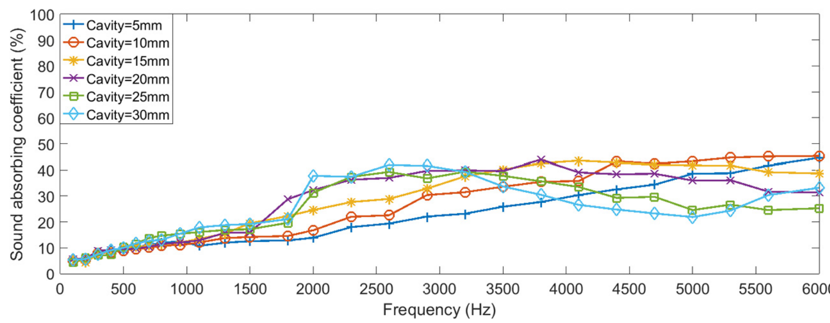

(e) The microperforated uncompressed porous metal

Fig. 3 (*continued*).

the microperforated spring steel panel, and the microperforated uncompressed porous metal, were measured for the sound absorbing coefficients with the cavities changing from 5 mm to 30 mm at the interval of 5 mm.

3. Results and discussions

Sound absorbing coefficients of the five samples with different cavities were summarized in Fig. 3. It could be observed that along with increase of length of the cavity, the peak absorption frequency decreased gradually for each sample, which was consistent with normal sound absorption principle of the porous metal and that of the microperforated panel respectively [12–17,21–24]. The peak absorption frequencies judged from the experimental data were summarized in Table 1.

It could be found that the peak absorption frequency of the microperforated spring steel panel was smallest with certain cavity, which indicated that it had relative better sound absorption performance in the low frequency range. In contrast, peak absorption frequency of the original porous metal was biggest with certain cavity, which indicated that its absorption advantage was in the high frequency range. It could also be discovered from distributions of the sound absorbing coefficients for the five samples that when length of the cavity was 30 mm, the sound absorbing coefficient rose again along with the increase of frequency in the high frequency range of 5000–6000 Hz, which indicated that the second peak absorption frequency would appear at the further higher frequency.

Comparisons of sound absorbing coefficients of the five samples with the same cavity were shown in Fig. 4, and the calculated average sound absorbing coefficients were summarized in Table 2. It could be found that sound absorption performance of the porous metal was remarkably improved through compression and microperforation. Especially when length of the cavity was 20 mm, average sound absorbing coefficient of the compressed and microperforated porous metal panel reached 59.69%, which was more than two times of that of the original porous metal and almost double of that of the microperforated spring steel panel. After compression, thickness of the sample was 0.5 mm, which indicated that resonance sound absorption was realized by the existing connected micropores in the compressed porous metal. That's why the sound absorption performance was obviously improved by the compression. However, these connected micropores were not standard holes, which indicated that their resonance sound absorption effects were smaller than those of the microperforated holes. That's why the sound absorption performance could be further improved through the microperforation. It could also be found that the sound absorption

Table 1
The peak absorption frequencies of the five samples with different cavities.

Sample	Cavity					
	5 mm	10 mm	15 mm	20 mm	25 mm	30 mm
Original porous metal	6000 Hz	5000 Hz	4400 Hz	4100 Hz	3800 Hz	3200 Hz
Compressed porous metal	6000 Hz	4400 Hz	3200 Hz	2600 Hz	2300 Hz	1800 Hz
Compressed and microperforated porous metal panel	5600 Hz	4700 Hz	3200 Hz	2600 Hz	2000 Hz	1800 Hz
Microperforated spring steel panel	4100 Hz	2900 Hz	2000 Hz	1800 Hz	1500 Hz	1300 Hz
Microperforated uncompressed porous metal	6000 Hz	6000 Hz	4100 Hz	3800 Hz	2600 Hz	2600 Hz

performance was decreased after microperforation of the uncompressed porous metal. We supposed there were two major reasons. Firstly, thickness of the uncompressed porous metal was 5 mm, which indicated the microperforation did not realize the resonance sound absorption similar with the microperforated panel. Secondly, the microperforation destroyed some porous structures, which resulted in decrease in the sound absorption performance. Thus, the microperforated uncompressed porous metal was eliminated in further study.

Meanwhile, it could be observed that the average sound absorbing coefficient did not always increase along with increase of the cavity, which indicated that there was an optimal cavity for the sample with a certain requirement of average sound absorbing coefficient. Supposing the requirement of sound absorbing coefficient was 50%, the satisfied frequency band for each sample could be judged from the experimental data (except microperforated uncompressed porous metal) and summarized in Fig. 5. It could be found that sound absorbing coefficient of the original porous metal with the varied cavity was all below 50% in the whole frequency range of 100–6000 Hz. After compression, there was an obvious improvement on the satisfied frequency band, which was further increased a bit after the microperforation. It could also be found that satisfied frequency band for the compressed porous metal and that for the compressed and microperforated porous metal reached their maximal values when length of the cavity was 20 mm, which were consistent with the results in Table 2. With respect to the microperforated spring steel panel, its satisfied frequency band was reduced gradually along with the increase of length of the cavity, which was consistent with the normal sound absorption principle for common microperforated panel absorber [12,13,23,24]. It could be concluded that relative to the original porous metal and the microperforated spring steel panel, compression and microperforation of the porous metal could remarkably improve its sound absorption performance, both in the average sound absorbing coefficient and the satisfied frequency band. Therefore, the compressed and microperforated porous metal panel absorber could be treated as an effective product for practical application in the noise reduction field.

4. Theoretical analysis

Sound absorption of the compressed and microperforated porous metal panel absorber was realized by superposition absorption effect of the porous structures and microperforated structures, which was different from sound absorption mechanism of the composite structures. For the composite structures, the sound absorption effects of each absorber acted sequentially, while those in the compressed and microperforated porous metal panel absorber acted simultaneously. Thus, these traditional methods, such as the transfer matrix method [25,26], equivalent circuit method [27], and impedance transfer method [28], were not suitable to predict sound absorbing coefficient of the compressed and microperforated porous metal panel absorber. Correction factors had been applied in the sound absorbing models to improve the prediction accuracy [18,21,29]. Therefore, a similar fourth-order polynomial function was treated as the coupling function to express superposition absorption effect of the two structures, which was obtained by data fitting. Meanwhile, sound absorbing coefficient of the original porous metal + cavity absorber was calculated based on the Johnson-Champoux-Allard model [22] and that of the microperforated panel + cavity absorber was derived based on the Maa's theory [23]. In this way, the preliminary theoretical analysis of sound absorbing coefficients of the compressed and microperforated porous metal panel absorber was conducted. According to transfer matrix method [25,26], sound absorbing coefficient α_M of the porous metal + cavity structure and that α_P of the microperforated panel + cavity structure could be calculated by the Eqs. (4) and (5), respectively. Here T_M is total transfer matrix of porous metal + cavity structure; T_P is total transfer matrix of microperforated panel + cavity structure; ρ is density of the air, 1.21 kg/m^3; c is the acoustic velocity in air, 343 m/s; P is transfer matrix of porous metal; M is transfer matrix of microperforated panel; S is transfer matrix of cavity. Meanwhile, Re() and Im() in the Eqs. (4) and (5) represent the real part and the imaginary part of one complex number, respectively.

$$\begin{cases} \alpha_M = \dfrac{4\,\mathrm{Re}\left(T_{M11}\cdot T_{M21}^{-1}\cdot\rho^{-1}c^{-1}\right)}{\left[1+\mathrm{Re}\left(T_{M11}\cdot T_{M21}^{-1}\cdot\rho^{-1}c^{-1}\right)\right]^2+\left[\mathrm{Im}\left(T_{M11}\cdot T_{M21}^{-1}\cdot\rho^{-1}c^{-1}\right)\right]^2} \\ T_M = \begin{bmatrix} T_{M11} & T_{M12} \\ T_{M21} & T_{M22} \end{bmatrix} = [P][S] \end{cases} \tag{4}$$

$$\begin{cases} \alpha_P = \dfrac{4\,\mathrm{Re}\left(T_{P11}\cdot T_{P21}^{-1}\cdot\rho^{-1}c^{-1}\right)}{\left[1+\mathrm{Re}\left(T_{P11}\cdot T_{P21}^{-1}\cdot\rho^{-1}c^{-1}\right)\right]^2+\left[\mathrm{Im}\left(T_{P11}\cdot T_{P21}^{-1}\cdot\rho^{-1}c^{-1}\right)\right]^2} \\ T_P = \begin{bmatrix} T_{P11} & T_{P12} \\ T_{P21} & T_{P22} \end{bmatrix} = [M][S] \end{cases} \tag{5}$$

According to the Johnson-Champoux-Allard model [22] and Maa's theory [23], transfer matrixes P, M, and S of the porous metal, the microperforated panel, and the cavity could be calculated by the Eqs. (6), (7), and (8), respectively. For the porous metal, k_p is the wave number in it; d_p is its thickness; Z_p is its characteristic impedance; these parameters can be calculated by the series of equations in the Eq. (9). For the microperforated panel, Z_s is its acoustic impedance, and it can be calculated by the series of equations in the Eq. (10). For the cavity, ω is angular frequency; c is acoustic velocity in air; D is length of the cavity. Meanwhile, j is symbol of imaginary number.

$$[P] = \begin{bmatrix} \cos(k_p d_p) & jZ_p \sin(k_p d_p) \\ jZ_p^{-1}\sin(k_p d_p) & \cos(k_p d_p) \end{bmatrix} \tag{6}$$

$$[M] = \begin{bmatrix} 1 & Z_s \\ 0 & 1 \end{bmatrix} \tag{7}$$

$$[S] = \begin{bmatrix} \cos\left(\omega D c^{-1}\right) & j\rho c\sin\left(\omega D c^{-1}\right) \\ j\rho^{-1}c^{-1}\sin\left(\omega D c^{-1}\right) & \cos\left(\omega D c^{-1}\right) \end{bmatrix} \tag{8}$$

$$\begin{cases} Z_p = \sqrt{\rho(\omega)K(\omega)} \\ k_p = \omega\sqrt{\dfrac{\rho(\omega)}{K(\omega)}} \\ \omega = 2\pi f \\ K(\omega) = \gamma P_0\left[\gamma-(\gamma-1)\left(1-N_u\left(j\dfrac{8\omega\rho P_r}{\sigma\phi}+N_u\right)^{-1}\right)\right]^{-1} \\ \rho(\omega) = \rho\left[1+\left(3^2+\dfrac{4\omega\rho}{\sigma\phi}\right)^{-0.5}-j\dfrac{\sigma\phi}{\omega\rho}\left(1+\dfrac{\omega\rho}{4\sigma\phi}\right)^{0.5}\right] \end{cases} \tag{9}$$

$$\begin{cases} Z_s = R+jX \\ R = \dfrac{32(\mu+\upsilon)\rho}{\varepsilon}\dfrac{t}{d^2}k_r \\ X = \dfrac{t\omega\rho}{\varepsilon}k_m \\ k_r = \sqrt{1+\dfrac{k^2}{32}}+\dfrac{\sqrt{2}}{8}k\dfrac{d}{t} \\ k_m = 1+\left(9+\dfrac{k^2}{2}\right)^{-0.5}+0.85\dfrac{d}{t} \\ k = \sqrt{\dfrac{\omega}{\mu+\upsilon}}\dfrac{d}{2} \end{cases} \tag{10}$$

In the Eq. (9), ω is also the angular frequency; $\rho(\omega)$ is the complex effective density; $K(\omega)$ is the complex effective bulk modulus; f is the acoustic frequency; γ is specific heat ratio of the air, 1.40; ρ is also density of the air; P_0 is static pressure of the air, $1.013 \cdot 10^5$ Pa; Pr is the Prandtl number, 0.71; N_u is the Nusselt number, 4.36; ϕ is porosity of the porous metal, 90%; σ is static flow resistivity of the porous metal, 9524 Pa·s·m^{-2} [18,21,30]. Meanwhile, In the Eq. (10), R and X are the real part and the imaginary part of the acoustic impedance of the microperforated panel; μ is viscosity coefficient of the air, 1.506 $\cdot\ 10^{-5}$ m^2/s; υ represents temperature conduction coefficient of the panel, $2.0 \cdot 10^{-5}$ m^2/s; ρ is also density of the air; ε is the perforating rate, 2.18%, which is obtained by the Eq. (3); k_r is acoustic resistance constant; ω is also angular frequency; k_m is acoustic mass constant; k is perforated panel constant; d is diameter of the hole, 0.75 mm; b is distance between the neighboring holes, 4.5 mm; t is thickness of the panel, 0.5 mm.

The fourth-order polynomial function P_{PM}, which was obtained by fitting the experimental data and shown in the Eq. (11), was treated as the coupling function and utilized to express the superposition absorption effect of porous structures and microperforated structures. In this way, sound absorbing coefficient α_{CP} of the proposed acoustic absorber could be calculated by the Eq. (12).

$$P_{PM} = \begin{bmatrix} 6.558 & 3.524 & 0.0404 & -4.729 \cdot 10^{-5} & -3.047 \cdot 10^{-6} \\ -2.348 & -0.6427 & -0.0027 & 2.852 \cdot 10^{-5} & 0 \\ 0.5343 & 0.034 & -4.04 \cdot 10^{-5} & 0 & 0 \\ -0.0209 & -4.346 \cdot 10^{-4} & 0 & 0 & 0 \\ 2.409 \cdot 10^{-4} & 0 & 0 & 0 & 0 \end{bmatrix} \tag{11}$$

$$\alpha_{CP} = \begin{bmatrix} 1 & \alpha_P & \alpha_P^2 & \alpha_P^3 & \alpha_P^4 \end{bmatrix} \cdot P_{PM} \cdot \begin{bmatrix} 1 & \alpha_M & \alpha_M^2 & \alpha_M^3 & \alpha_M^4 \end{bmatrix}' \tag{12}$$

Taking actual parameters of the proposed acoustic absorber to the constructed semi-empirical model in the Eq. (12), comparisons of the experimental data and the theoretical data were shown in Fig. 6. It

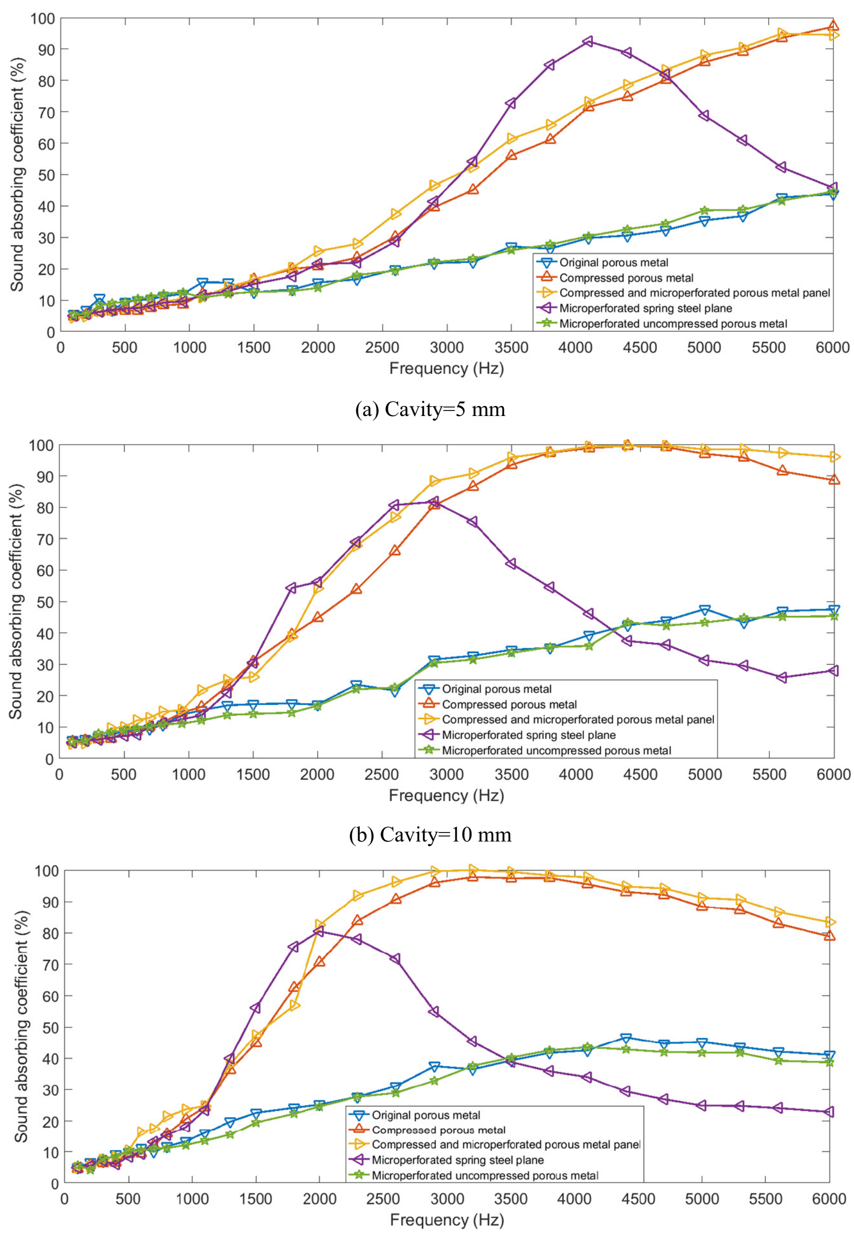

(a) Cavity=5 mm

(b) Cavity=10 mm

(c) Cavity=15 mm

Fig. 4. Comparisons of sound absorbing coefficients of the five samples with the same cavity.

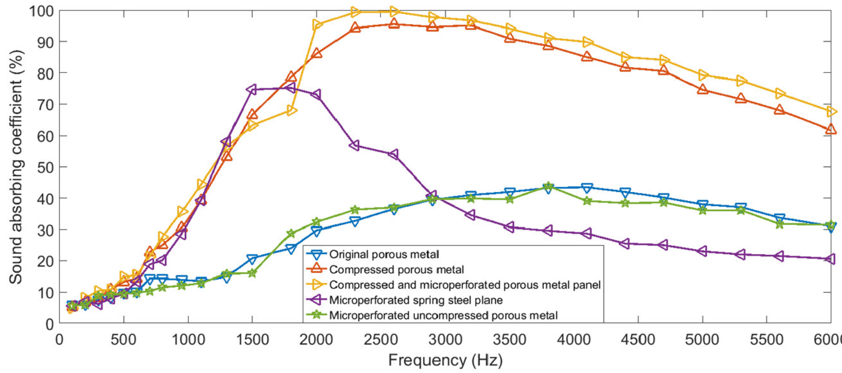

(d) Cavity=20 mm

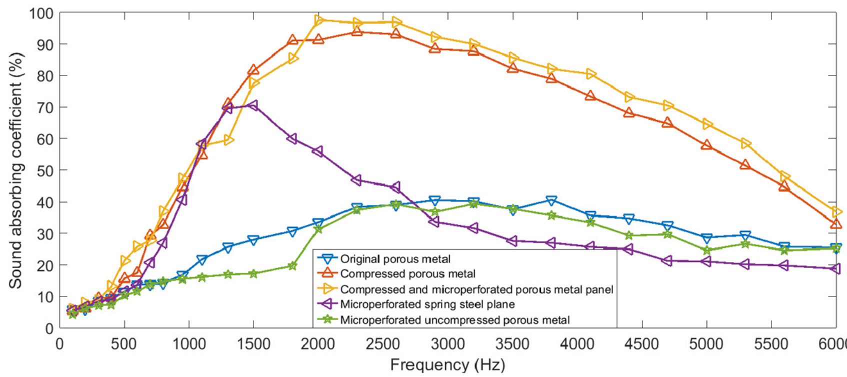

(e) Cavity=25 mm

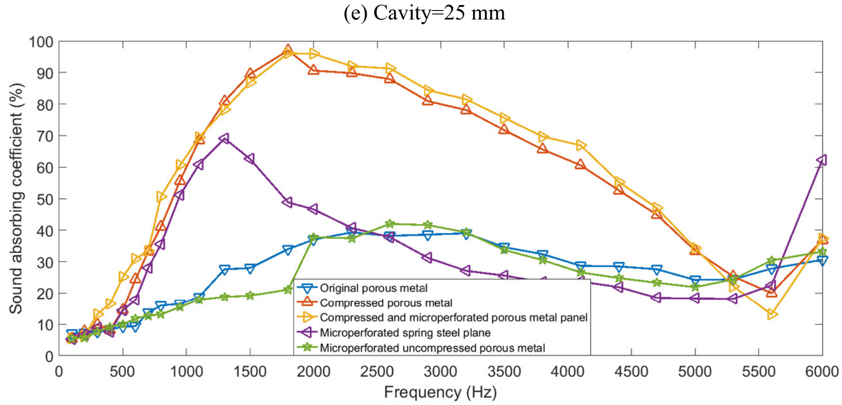

(f) Cavity=30 mm

Fig. 4 (*continued*).

could be observed that consistency of the experimental data and the theoretical data was excellent, especially when the cavity was 20 mm. The total departure of the regressive average value R^2 was used to quantitatively evaluate prediction accuracy of the model, and it could be obtained by Eq. (13) [18]. Here α_{ei} was actual sound absorption coefficient obtained by experiment; N was numbers of the measured frequency points, 27. It could be calculated that values of R^2 for the compressed and microperforated porous metal panel absorber were

Table 2
The average sound absorbing coefficients of the five samples with different cavities.

Sample	Cavity					
	5 mm	10 mm	15 mm	20 mm	25 mm	30 mm
Original porous metal	20.03%	24.16%	26.35%	25.70%	25.51%	24.23%
Compressed porous metal	36.69%	51.08%	55.97%	57.14%	54.72%	50.91%
Compressed and microperforated porous metal panel	38.85%	54.16%	58.87%	59.69%	57.36%	53.31%
Microperforated spring steel panel	34.77%	33.53%	32.41%	31.49%	30.38%	30.91%
Microperforated uncompressed porous metal	20.12%	23.13%	25.04%	25.05%	22.67%	22.77%

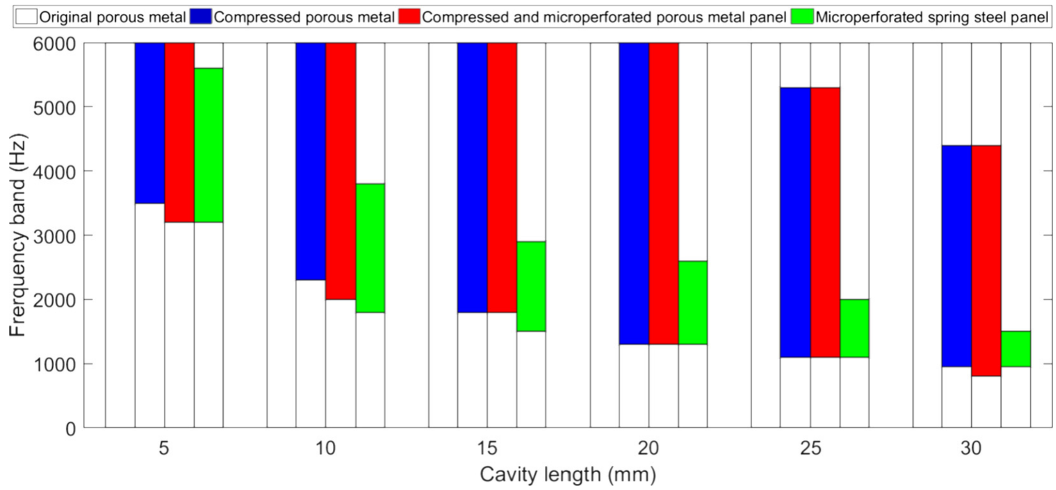

Fig. 5. The satisfied frequency bands with the requirement of sound absorbing coefficient at 50%.

0.989, 0.9958, 0.9986, 0.9987, 0.9947, and 0.9809 corresponding to the cavities of 5 mm, 10 mm, 15 mm, 20 mm, 25 mm, and 30 mm, which verified effectiveness of the semi-empirical model.

$$R^2 = 1 - \frac{\sum_{i=1}^{N} (\alpha_{ei} - \alpha_{CPi})^2}{\sum_{i=1}^{N} \alpha_{ei}^2} \tag{13}$$

Through the constructed semi-empirical model, evolution of the calculated average sound absorbing coefficient of the proposed acoustic absorber with different cavities was shown in Fig. 7. It could be found that when the investigated frequency range was 100–6000 Hz (the blue solid line in Fig. 7), there were four maximal values (corresponded to the cavities of 20 mm, 49 mm, 76 mm, and 95 mm) and three minimal values (corresponded to the cavities of 29 mm, 56 mm, and 86 mm) in length range of the cavity 1–100 mm. these extremums were generated by the continued appearance of higher order resonance frequency for the proposed acoustic absorber along with increase of length of the cavity, which could also be judged from distributions of sound absorbing coefficients in Figs. 3, 4(f), and 6(f). Meanwhile, it could be observed that maximal value of the average sound absorbing coefficient was gradually increased from 56.58% (corresponding to the cavity of 20 mm) to 63.15% (corresponding to the cavity of 95 mm), which was consistent with the universal sound absorption principle of normal microperforated panel [12,13,23,24]. The validation of prediction reliability of the averaged sound absorbing coefficient was conducted by measuring the proposed acoustic absorber when length of the cavity was 60 mm, and the result was shown in Fig. 8. The theoretical data was consistent with the experimental data, and the calculated actual average sound absorbing coefficient was 60.08%, which was close to that of 59.41% in theory and could further validate the effectiveness and accuracy of the constructed semi-empirical model. It was known that there would be more absorption peaks along with increase of length of the cavity [12,13,23,24]. It could be judged from the experimental data for the compressed and microperforated porous metal panel with cavity of 30 mm in Fig. 4(f) that the first resonance absorption frequency was 1800 Hz, and the second resonance absorption frequency would appear when the cavity was larger. Therefore, when length of the cavity was 60 mm in Fig. 8, 900 Hz was the first resonance absorption frequency and 3500 Hz was the second resonance absorption frequency. It could be predicted that the third resonance absorption frequency would appear when length of the cavity was larger. There was also another absorption peak at 1600 Hz in Fig. 8, and its corresponding wavelength was 214 mm, which was close to four times of length of the cavity 60 mm. We supposed that there was an absorption peak when one quarter of the wavelength was close to length of the cavity. The average sound absorbing coefficient was not only affected by the given length of the cavity, but also be influenced by the investigated frequency range, which could be judged from the evolution of average sound absorbing coefficients when the investigated frequency range was 2000–6000 Hz (red dashed line in Fig. 7) and when the investigated frequency range was 100–2000 Hz (purple dotted line in Fig. 7).

The optimal length of the cavity for certain requirements could be calculated by the constructed semi-empirical model. Noise frequency ranges of one given air compressor in the working condition was 2000–5000 Hz, and the requirement of noise reduction was that the sound absorbing coefficient in this frequency range should exceed 80%, which could be summarized in Eq. (14). According to the constructed semi-empirical model in Eq. (12), it could be derived that the optimal length of the cavity was 17.91 mm. Owing to control accuracy of the used AWA6128A detector, the optimal length of the cavity was selected 18 mm by approximating, and the corresponding experimental results and theoretical results were shown in Fig. 9. It could be observed that the obtained optimal results were exactly satisfied to the requirement. In the second case, requirement of the noise reduction in one workshop was that the average sound absorbing coefficient exceeded 55% in the frequency range of 100–2000 Hz, which could be expressed in Eq. (15). The calculated optimal length of the cavity in theory was 47.86 mm, which was approximated to 48 mm in actual experiment. Judging from the experimental result and the theoretical result in Fig. 10 it could be found that these two data were consistent. The actual average sound absorbing coefficient was 56.61%, which met the requirement and was close to the theoretical average sound absorbing coefficient 55.39%. It could also be found that when length of the cavity was 48 mm, the first resonance absorption frequency was 1100 Hz and the second resonance absorption frequency was 4300 Hz. The another absorption peak was round 2000 Hz, and its corresponding wavelength was 171.5 mm. One quarter of the wavelength was 43 mm, which was close to length of the cavity 48 mm. The two replication experiments indicated that the compressed and microperforated porous metal panel absorber was efficient in noise reduction and the optimal acoustic absorber could be achieved according to the constructed model.

$$D^* = \min\{D | \alpha_{CP}(f) \geq 80\%, f \in [2000\text{Hz}, 5000\text{Hz}]\} \tag{14}$$

$$D^{**} = \min\{D | aver(\alpha_{CP}(f)) \geq 55\%, f \in [100\text{Hz}, 2000\text{Hz}]\} \tag{15}$$

5. Micromorphology

The samples were further investigated by scanning electron microscope (JSM-6360LV (JEOL Ltd., Tokyo, Japan)), and their corresponding surface morphologies were shown in Fig. 11, which aimed to study the sound absorption performance from the microstructure. It could be observed from Fig. 11(a) that there were standard pore structures in original porous metal [21], and these pore structures were destroyed by the compression [18], as shown in Fig. 11(b). After further microperforation, the compressed and microperforated porous metal panel was obtained, as shown in Fig. 11(c). Compared with the microperforated spring steel panel in Fig. 11(d), it could be observed that the compressed and microperforated porous metal panel was not solid, and there were many reticular gaps in its surface and interior. Therefore, besides the resonance absorption effect obtained by the micropore, there were also viscous effect and heat conduction in sound absorption process of the compressed and microperforated porous metal panel absorber, which were realized by these reticular gaps. This superposition absorption effect was more obvious in the high frequency range, which could also be judged from comparisons of the sound absorbing coefficients in Fig. 4, because porous structure and reticular gap was more effective at sound absorption in the high frequency range. After compression, porosity of the sample was decreased and its static flow resistivity was increased, because thickness of the sample

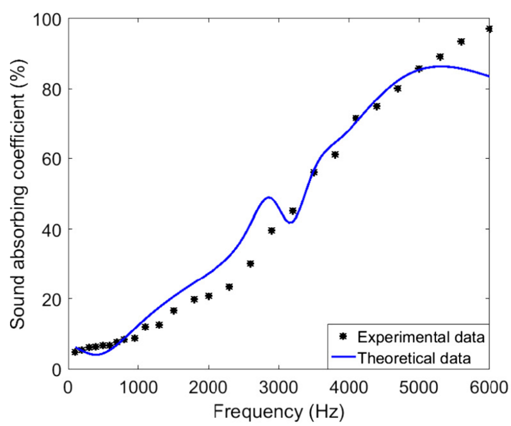

(a) Cavity=5 mm

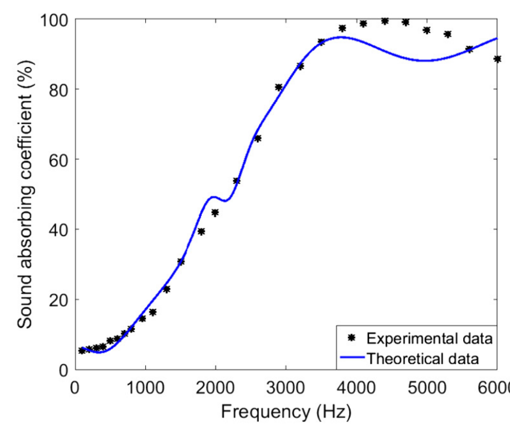

(b) Cavity=10 mm

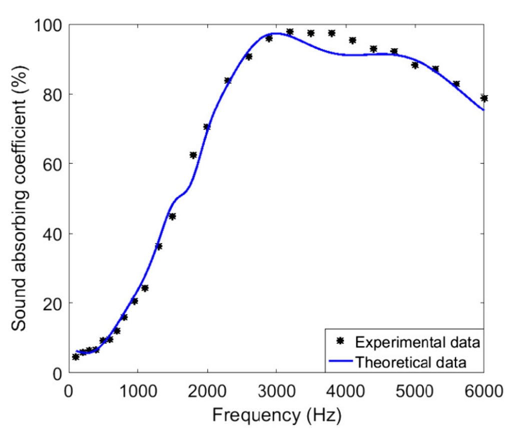

(c) Cavity=15 mm

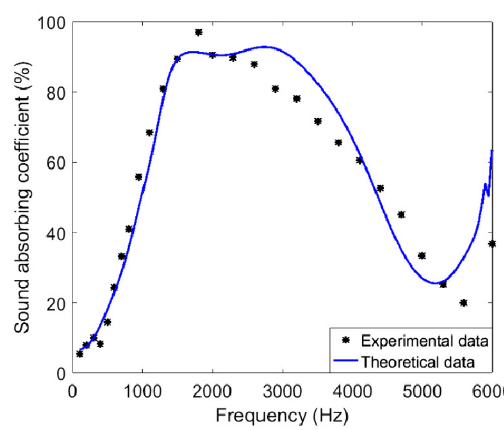

(d) Cavity=20 mm

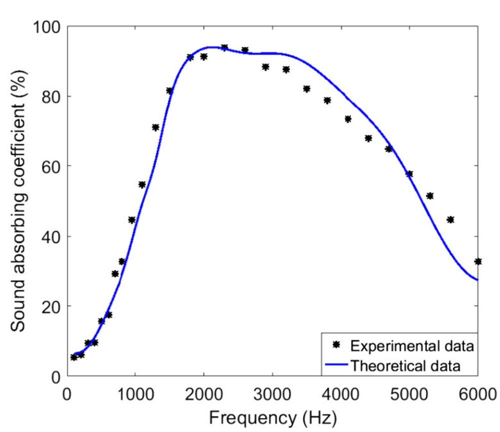

(e) Cavity=25 mm

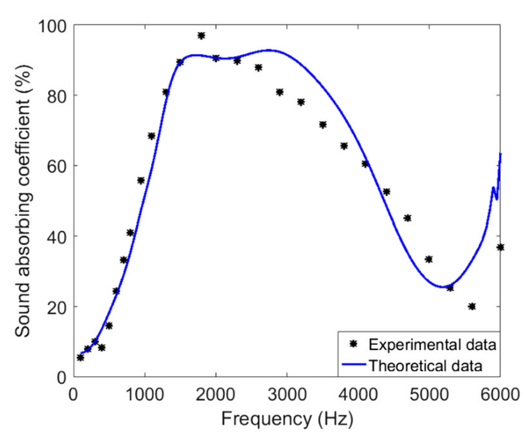

(f) Cavity=30 mm

Fig. 6. Comparisons of the experimental data and theoretical data for the proposed acoustic absorber.

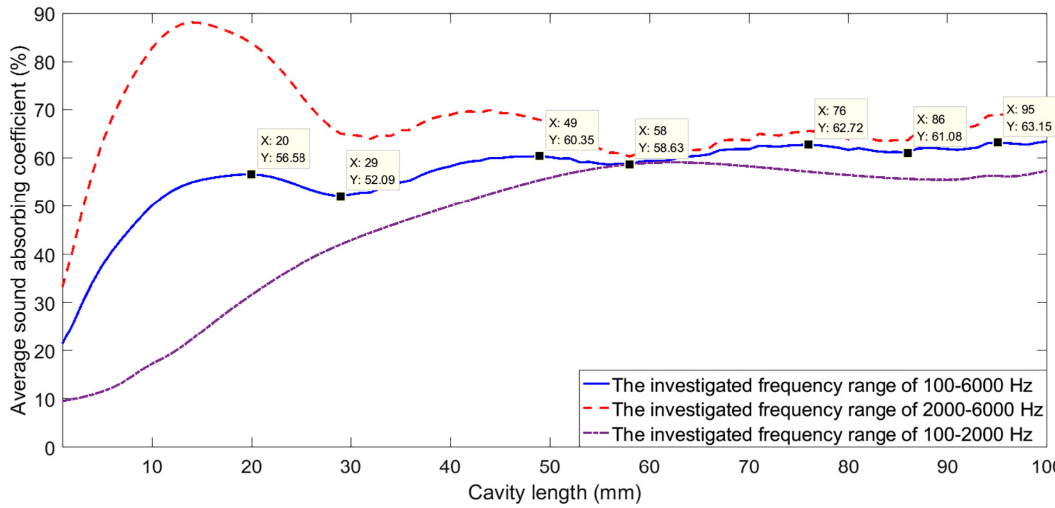

Fig. 7. Evolutions of average sound absorbing coefficients along with increase of length of the cavity.

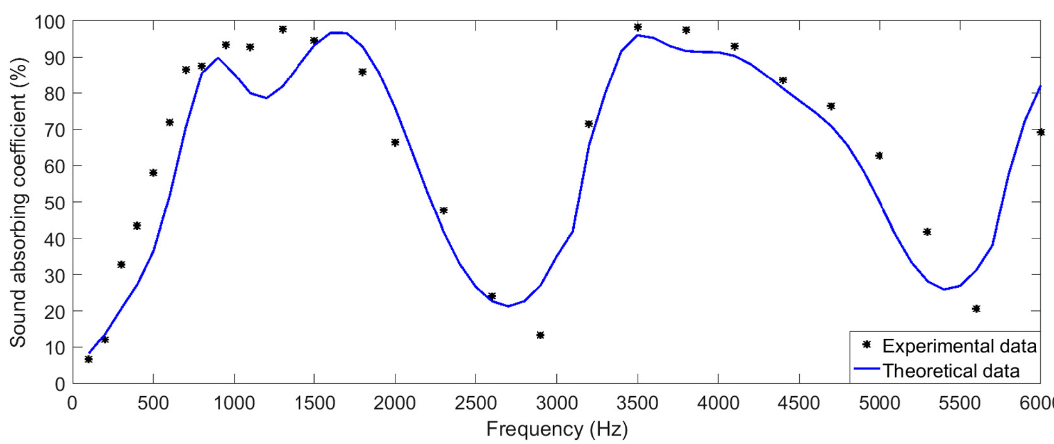

Fig. 8. Comparison of the theoretical data and the experimental data for the proposed compressed and microperforated porous metal panel absorber with length of the cavity 60 mm.

was reduced by the compression, which resulted in the deviations between actual sound absorption performance and theoretical sound absorption performance.

In order to further study microstructure of the compressed and microperforated porous metal panel, its cross-sectional morphologies were achieved by inclining the sample 30°, and the obtained results were shown in Fig. 12. It could be observed that side wall of the micropore was also not solid and there were some irregular micro-vias. These irregular micro-vias were considered as one reason for the decrease of sound absorbing coefficient of the proposed acoustic absorber relative

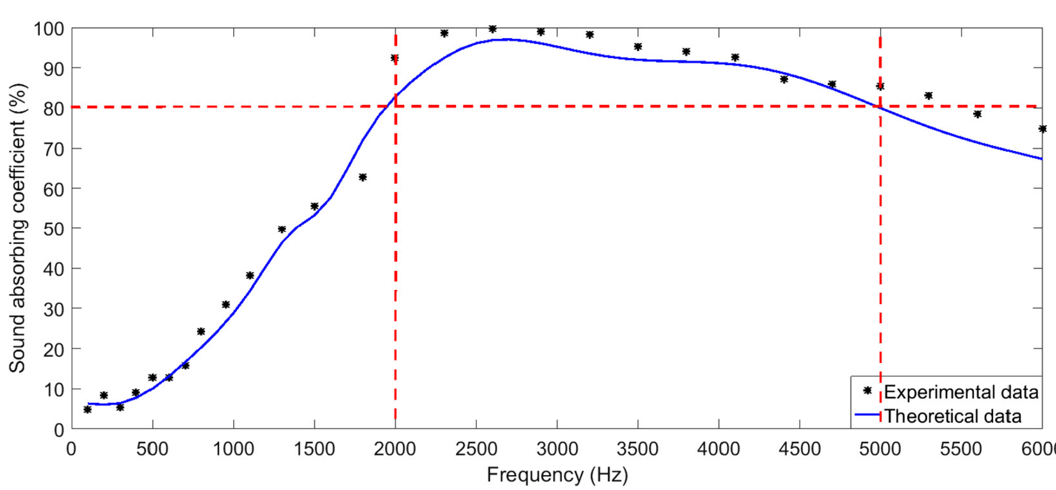

Fig. 9. The optimal compressed and microperforated porous metal panel absorber for the sound absorbing coefficient beyond 80% in the frequency range of 2000–5000 Hz.

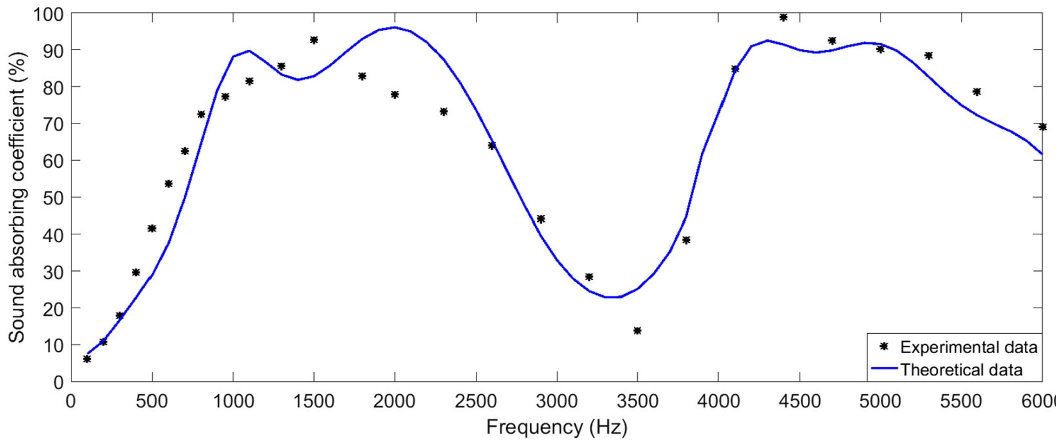

Fig. 10. The optimal compressed and microperforated porous metal panel absorber for the average sound absorbing coefficient beyond 55% in the frequency range of 100–2000 Hz.

to that of the microperforated spring steel panel in some frequency points, especially when length of the cavity was small, which could also be judged from the results in Fig. 4. In addition, the compressed microperforated porous metal panel was a highly resistive structure with a quarter-wavelength resonance at a much higher frequency than the Helmholtz-type resonance of the microperforated spring steel panel, and these resonances got close to each other when length of the cavity was larger, which also resulted in the decrease of its sound absorbing coefficient in some frequency points.

6. Conclusions

Sound absorption performances of the five acoustic absorbers with different cavity were investigated, which included original porous

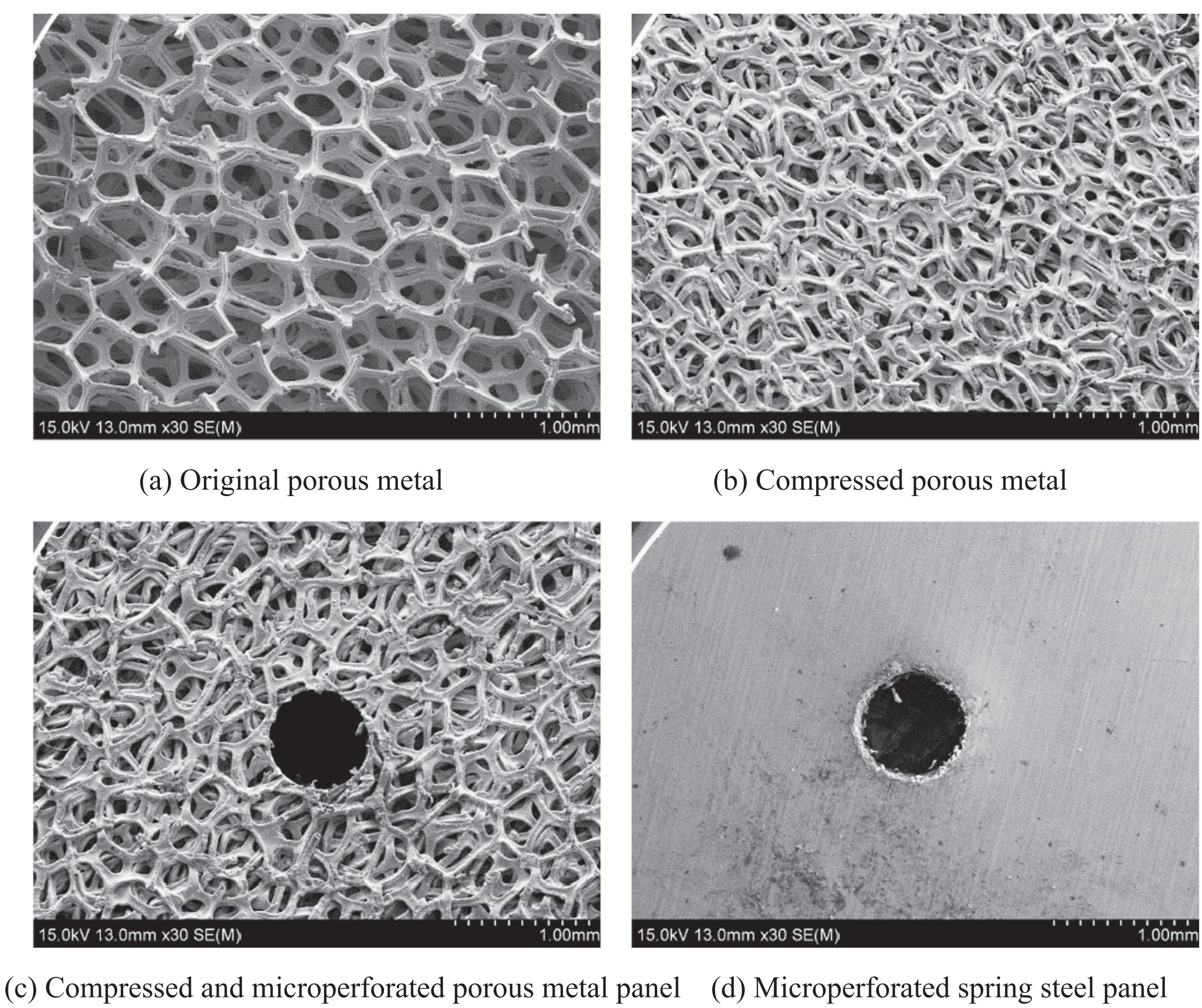

Fig. 11. Surface morphologies of the investigated samples obtained by scanning electron microscope.

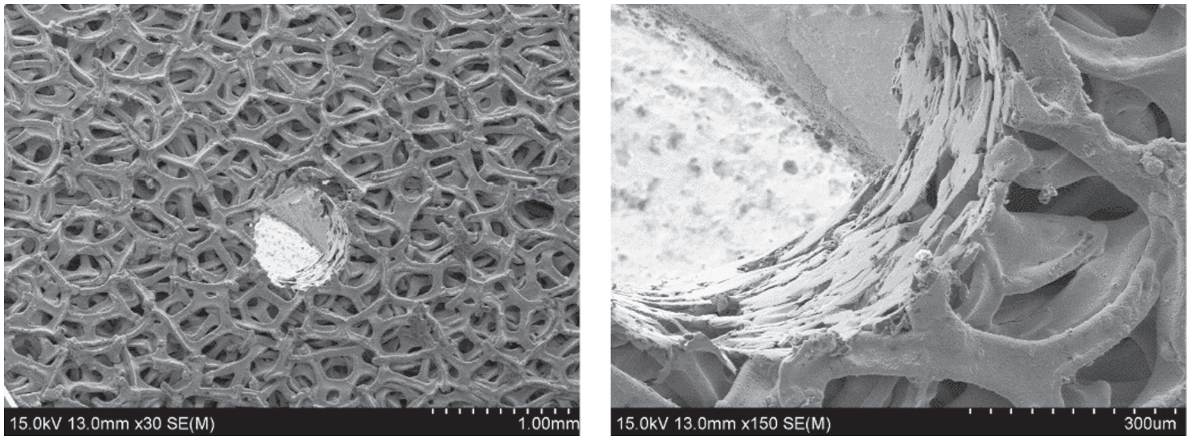

(a) With low magnification of ×30 (b) With high magnification of ×150

Fig. 12. Cross-sectional morphologies of the compressed and microperforated porous metal panel.

metal, compressed porous metal, compressed and microperforated porous metal panel, microperforated spring steel panel, and microperforated uncompressed porous metal. By the material fabrication, experimental measurement, results discussion, theoretical analysis, and micromorphology investigation, the following conclusions could be obtained in this study.

(1) Novel acoustic absorbers were developed by the compression and microperforation of the porous metal, and original porous metal and microperforated spring steel panel were treated as the contrast. The evolution trends of sound absorbing coefficients of the five investigated acoustic absorbers with different lengths of the cavity were consistent with normal sound absorption principle of the porous metal absorber and that of the microperforated panel absorber, respectively.
(2) With same length of the cavity, sound absorption performance could be obviously improved by compression and microperforation of the porous metal. Especially when length of the cavity was 20 mm, average sound absorbing coefficient of the compressed and microperforated porous metal panel absorber in the frequency range 100–6000 Hz was 59.69%, which was superior to that 25.70% of the original porous metal absorber and that 31.49% of the microperforated spring steel panel absorber.
(3) A fourth-order polynomial function was treated as the coupling function to express superposition absorption effect of the reticular gaps and micropore in the compressed and microperforated porous metal panel absorber. Comparisons of the theoretical data and experimental data proved veracity and reliability of the semi-empirical model. Two replication experiments with given requirements proved that the compressed and microperforated porous metal panel absorber was effective in the noise reduction and the optimal acoustic absorber could be achieved according to the constructed model.
(4) Surface morphologies of the investigated samples obtained by the scanning electron microscope showed that the pore structures in the original porous metal was compressed to the reticular gaps, and there were irregular micro-vias on the micropore fabricated by the further microperforation. Micromorphology of the compressed and microperforated porous metal panel could give the intuitive explanations to the improvement of its sound absorption performance.

The proposed acoustic absorber obtained by compression and microperforation of the porous metal can obtain excellent sound absorption performance, and it can be optimized for certain requirement by the constructed semi-empirical model, which will be propitious to promote practical application of the proposed acoustic absorber in the noise reduction field.

CRediT authorship contribution statement

Panfeng Bai: Conceptualization, Data curation, Formal analysis, Writing - original draft, Writing - review & editing. **Xiaocui Yang:** Data curation, Formal analysis. **Xinmin Shen:** Conceptualization, Formal analysis, Funding acquisition, Methodology, Supervision, Writing - original draft. **Xiaonan Zhang:** Data curation, Funding acquisition, Supervision. **Zhizhong Li:** Investigation, Methodology, Validation. **Qin Yin:** Investigation, Validation. **Guoliang Jiang:** Writing - review & editing. **Fei Yang:** Writing - review & editing.

Acknowledgements

This work was supported by a grant from National Natural Science Foundation of China (Grant No. 51505498), a grant from Natural Science Foundation of Jiangsu Province (Grant No. BK20150714), and a grand from National Key R & D Program of China (Grant No. 2016YFC0802900). Xinmin Shen was grateful for support from the Hong Kong Scholars Program (No. XJ2017025).

References

[1] M.S. Hammer, T.K. Swinburn, R.L. Neitzel, Environmental noise pollution in the United States: developing an effective public health response, Environ. Health Perspect. 122 (2) (2014) 115–119.
[2] M.R. Mehdi, M. Kim, J.C. Seong, M.H. Arsalan, Spatio-temporal patterns of road traffic noise pollution in Karachi, Pakistan, Environ. Int. 37 (1) (2011) 97–104.
[3] C.R. Kight, J.P. Swaddle, How and why environmental noise impacts animals: an integrative, mechanistic review, Ecol. Lett. 14 (2011) 1052–1061.
[4] C.D. Francis, J.R. Barber, A framework for understanding noise impacts on wildlife: an urgent conservation priority, Front. Ecol. Environ. 11 (6) (2013) 305–313.
[5] G.C. Ma, P. Sheng, Acoustic metamaterials: from local resonances to broad horizons, Sci. Adv. 2 (2) (2016), e1501595. .
[6] G.C. Ma, M. Yang, S.W. Xiao, Z.Y. Yang, P. Sheng, Acoustic metasurface with hybrid resonances, Nat. Mater. 13 (2014) 873–878.
[7] K.H. Matlack, A. Bauhofer, S. Krödel, A. Palermo, C. Daraio, Composite 3D-printed metastructures for low-frequency and broadband vibration absorption, PNAS 113 (30) (2016) 8386–8390.
[8] X.Z. Zhao, G.Q. Liu, C. Zhang, D. Xia, Z.M. Lu, Fractal acoustic metamaterials for transformer noise reduction, Appl. Phys. Lett. 113 (2018) 074101.
[9] S. Kumar, P. Bhushan, S. Bhattacharya, Ultrathin Ashoka Chakra like acoustic metastructure as a sound absorber, J. Acoust. Soc. Am. 143 (3) (2018) 1714.

[10] X.L. Wang, X.D. Luo, H. Zhao, Z.Y. Huang, Acoustic perfect absorption and broadband insulation achieved by double-zero metamaterials, Appl. Phys. Lett. 112 (2018) 021901.
[11] M. Yang, S.Y. Chen, C.X. Fu, P. Sheng, Optimal sound-absorbing structures, Mater. Horiz. 4 (2017) 673–680.
[12] X.W. Xu, H.X. Wang, Y. Sun, J.Q. Han, R.Z. Huang, Sound absorbing properties of perforated composite panels of recycled rubber, fiberboard sawdust, and high density polyethylene, J. Clean. Prod. 187 (2018) 215–221.
[13] F. Bucciarelli, G.P. Malfense Fierro, M. Meo, A multilayer microperforated panel prototype for broadband sound absorption at low frequencies, Appl. Acoust. 146 (2019) 134–144.
[14] P.S. Liu, H.B. Qing, H.L. Hou, Primary investigation on sound absorption performance of highly porous titanium foams, Mater. Des. 85 (2015) 275–281.
[15] A.J. Otaru, H.P. Morvan, A.R. Kennedy, Modelling and optimisation of sound absorption in replicated microcellular metals, Scr. Mater. 150 (2018) 152–155.
[16] T. Bravo, C. Maury, C. de la Colina, Absorption of thin micro-perforated partitions lined with anisotropic fibrous materials, J. Acoust. Soc. Am. 141 (5) (2017) 3872.
[17] Z.Q. Liu, J.X. Zhan, M. Fard, J.L. Davy, Acoustic measurement of a 3D printed microperforated panel combined with a porous material, Measurement 104 (2017) 233–236.
[18] P.F. Bai, X.M. Shen, X.N. Zhang, X.C. Yang, Q. Yin, A.X. Liu, Influences of compression ratios on sound absorption performance of porous nickel-iron alloy, Metals 8 (7) (2018) 539.
[19] H.B. Zhang, Y.H. Ye, R.Q. Shen, C.B. Ru, Y. Hu, Effect of bubble behavior on the morphology of foamed porous copper prepared via electrodeposition, J. Electrochem. Soc. 160 (2013) D441–D445.
[20] Y.J. Qian, D.Y. Kong, J.T. Fei, A note on the fabrication methods of flexible ultra microperforated panels, Appl. Acoust. 90 (2015) 138–142.
[21] X.C. Yang, K. Peng, X.M. Shen, X.N. Zhang, P.F. Bai, J. Xu, Geometrical and dimensional optimization of sound absorbing porous copper with cavity, Mater. Des. 131 (2017) 297–306.
[22] J.F. Allard, Y. Champoux, New empirical equations for sound propagation in rigid frame fibrous materials, J. Acoust. Soc. Am. 91 (6) (1992) 3346–3353.
[23] D.Y. Maa, Theory and design of microperforated panel sound-absorbing constructions, Sci. Sinica 18 (1) (1975) 55–71.
[24] D.Y. Maa, Potential of microperforated panel absorber, J. Acoust. Soc. Am. 104 (5) (1998) 2861–2866.
[25] X.B. Cai, J. Yang, G.K. Hu, Optimization on microlattice materials for sound absorption by an integrated transfer matrix method, J. Acoust. Soc. Am. 137 (4) (2015) EL334–EL339.
[26] X.C. Yang, P.F. Bai, X.M. Shen, S. To, L. Chen, X.N. Zhang, Q. Yin, Optimal design and experimental validation of sound absorbing multilayer microperforated panel with constraint conditions, Appl. Acoust. 146 (2019) 334–344.
[27] R. Pieren, K. Heutschi, Modelling parallel assemblies of porous materials using the equivalent circuit method, J. Acoust. Soc. Am. 137 (2) (2015) EL131–EL136.
[28] J. Zou, Y. Shen, J.B. Yang, X.J. Qiu, A note on the prediction method of reverberation absorption coefficient of double layer micro-perforated membrane, Appl. Acoust. 67 (2) (2006) 106–111.
[29] N. Kino, Further investigations of empirical improvements to the Johnson–Champoux–Allard model, Appl. Acoust. 96 (2015) 153–170.
[30] N. Kino, T. Ueno, Improvements to the Johnson-Allard model for rigid-framed fibrous materials, Appl. Acoust. 68 (2007) 1468–1484.